Received: 23 November 2020 | Revised: 19 April 2021 | Accepted: 22 April 2021

DOI: 10.1002/ppp.2117

RESEARCH ARTICLE

WILEY

Rock glacier inventory of the western Nyainqêntanglha Range, Tibetan Plateau, supported by InSAR time series and automated classification

Eike Reinosch[1] | Markus Gerke[1] | Björn Riedel[1] | Antje Schwalb[2] | Qinghua Ye[3] | Johannes Buckel[4]

[1]Institute of Geodesy and Photogrammetry, Technische Universität Braunschweig, Braunschweig, Germany

[2]Institute of Geosystems and Bioindication, Technische Universität Braunschweig, Braunschweig, Germany

[3]Institute of Tibetan Plateau Research (ITP), Chinese Academy of Sciences (CAS), Beijing, China

[4]Institute for Geophysics and Extraterrestrial Physics, Technische Universität Braunschweig, Braunschweig, Germany

Correspondence
Eike Reinosch, Institute of Geodesy and Photogrammetry, Technische Universität Braunschweig, Bienroder Weg 81, 38106, Braunschweig, Germany.
Email: e.reinosch@tu-braunschweig.de

Funding information
Deutsche Forschungsgemeinschaft, Grant/Award Number: DFG grant 317,513,741/GRK 2309

Abstract

The western Nyainqêntanglha Range on the Tibetan Plateau reaches an elevation of 7,162 m and is characterized by an extensive periglacial environment under semi-arid climatic conditions. Rock glaciers play an important part of the water budget in high mountain areas and recent studies suggest that they may even act as climate-resistant water storages. In this study we present the first rock glacier inventory of this region containing 1,433 rock glaciers over an area of 4,622 km. To create the most reliable inventory we combine manually created rock glacier outlines with an automated classification approach. The manual outlines were generated based on surface elevation data, optical satellite imagery and a surface velocity estimation. This estimation was generated via InSAR time series analysis with Sentinel-1 data from 2016 to 2019. Our pixel-based automated classification was able to correctly identify 87.8% of all rock glaciers in the study area at a true positive rate of 69.5%. In total, 65.9% of rock glaciers are classified as transitional with surface velocities of 1–10 cm/yr. In total, 18.5% are classified as active with higher velocities of up to 87 cm/yr. The southern windward side of the mountain range contains more numerous and more active rock glaciers. We attribute this to higher moisture availability supplied by the Indian Monsoon.

KEYWORDS
rock glacier, inventory, InSAR, Tibetan Plateau, time series, Nyainqêntanglha Range

1 | INTRODUCTION

1.1 | Importance of rock glacier inventories

Rock glaciers are lobate or tongue-shaped landforms developing through gravity-driven creep of frozen debris and interstitial ice.[1–3] Rock glaciers play an important part in the water budget of high mountain areas.[4] Their capacity to store fresh water in winter makes them important sources of fresh water in summer for semi-arid and arid regions such as the central Andes and the Sierra Nevada.[5–9] Recent studies have highlighted the importance of rock glaciers to act as temperature- and climate-resistant water storages and buffers to hydrological seasonality due to the insulating effect of the debris.[4,10,11] Their importance to mountain hydrology is

likely to increase over the coming decades due to global glacial retreat.[12] Rock glacier inventories have been used to estimate the regional lower permafrost limit,[13,14] though subsurface ice may still be found in favorable conditions at much lower elevations.[15] Rock glaciers have displayed accelerated motion rates over the past decades in the European Alps, northern Norway, the Carpathian Mountains, and the Tien Shan.[16–18] This can potentially lead to hazardous mass wasting processes due to destabilizing rock glaciers.[19,20] The potential of rock glaciers to act as climate-resistant water storages combined with the importance of the Tibetan Plateau (TP) as a source of fresh water to ~1.65 billion people in Asia[21] and the amplified warming effect of climate change on the TP[22] emphasize the necessity to study rock glacier distribution on the TP.

1.2 | Rock glacier morphology

The precise definition of what constitutes a rock glacier and its potential origins have been discussed but remain contested. Rock glaciers are described as the visible expression of cumulative deformation by long-term creep of ice/debris mixtures under permafrost conditions.[23] Rock glaciers may develop in periglacial, paraglacial, or glacial environments.[24] They may exist in areas where permafrost is unlikely outside the rock glaciers themselves when gravity-driven creep extends the landform beyond the expected periglacial zone.[25] They are typical landforms of high mountain environments and can extend up to multiple kilometers in length and several hundred meters to a kilometer in width. Rock glacier debris often originates from avalanche processes and rock falls, which can be triggered by continuous headwall weathering, sudden heavy precipitation, or earthquakes.[3] Rock glaciers may also develop from frozen moraines or debris-covered glaciers.[10,26,27] The latter often include glacial ice within the rock glacier body. Rock glaciers developing without a connection to a glacier form ice within the debris by freezing rain or melt water and/or by burying accumulations of snow and ice.[28]

1.3 | Rock glacier activity

Rock glaciers that contain ice are categorized as active if they display motion and as inactive if they are unmoving. Unmoving rock glaciers without ice in their bodies are referred to as fossil or relict rock glaciers.[1] Active rock glaciers often display horizontal velocities of centimeters to decimeters per year but may reach velocities of several meters per year.[16,18] Velocities are influenced by changes of ground temperature as well as moisture availability, which may accelerate or decelerate a rock glacier on a decadal scale.[29–32] Rock glaciers also display strong seasonal variations in their surface motion in many cases, with higher velocities in summer and autumn compared to winter and spring.[33–35]

1.4 | Creating rock glacier inventories

The spatial coverage and comparability of rock glacier inventories are lagging behind inventories of glaciers on a global scale.[12] This is due to a number of reasons including: (a) the necessity of high-resolution satellite data to identify rock glaciers and to distinguish them from surrounding landforms; (b) the difficulty in judging their status of activity and their ice content; and (c) the subjectivity of identifying and outlining rock glaciers and the dependency on the analyst's experience to distinguish them from similar landforms such as debris-covered glaciers and ice-cored glacial moraines.[26,36] The availability of freely accessible global map providers such as Bing Map, Google Maps, or Zoom Earth are alleviating issue (a). However, remote areas often display lower temporal and spatial data coverage compared to urban centers and the positional accuracy may vary. Microwave remote sensing data and Interferometric Synthetic Aperture Radar (InSAR) techniques have been applied successfully to determine rock glacier activity in some large-scale inventories in recent years (Table 1). This addresses issue (b). InSAR techniques allow monitoring surface motion on the order of a few millimeters to decimeters per year depending on the technique used, the wavelength and the revisit time of the satellite constellation.[37] Issue (c) has led to problems in the comparability of rock glacier inventories of different regions due to varying inventorying methodologies. Identifying a landform as a rock glacier and subsequently manually creating its outline is subjective. This leads to large variabilities in both the number of rock glaciers and their surface areas when comparing the rock glacier inventories created by different analysts.[36] The recently formed action group on "Rock glacier inventories and kinematics" of the International Permafrost Association (IPA) aims to address these issues. They explore the feasibility of developing widely accepted standard guidelines for inventorying rock glaciers on a global scale, including information on their kinematics.[38,39] Furthermore, varying techniques to detect rock glaciers automatically based on remote sensing data have achieved promising results.[40–44] In this study we follow the practical guidelines of the IPA action group to generate a manual inventory and compare it to automated classification results to work towards a global rock glacier inventory.

1.5 | Purpose of this study

We present an inventory of actively moving rock glaciers within the western Nyainqêntanglha Range on the southeastern TP (Figure 1). We combine a manual approach with an automated classification algorithm to generate an exhaustive rock glacier inventory. Following the IPA guidelines ensures the comparability with future rock glacier inventories following these guidelines. Combining the manual approach with a semi-automated classification increases the reliability of the inventory. This inventory is the first of its kind in this mountain range and will help to fill the gaps

TABLE 1 Rock glacier inventories with velocity information based on differential interferometric synthetic aperture radar (DInSAR) techniques

Region	Number of rock glaciers	Period of InSAR velocity data	InSAR technique
Tien Shan[18]	551	1998 to 2018	DInSAR
Dry Andes[7]	2,116	2014 to 2017	DInSAR
Tien Shan[45]	261	2007 to 2009	DInSAR
Swiss Alps[46]	908	1991 to 2012	DInSAR
Sierra Nevada[47]	59	2007 to 2008	DInSAR
Swiss Alps[48]	Not specified (~30)	1995 to 1999	DInSAR

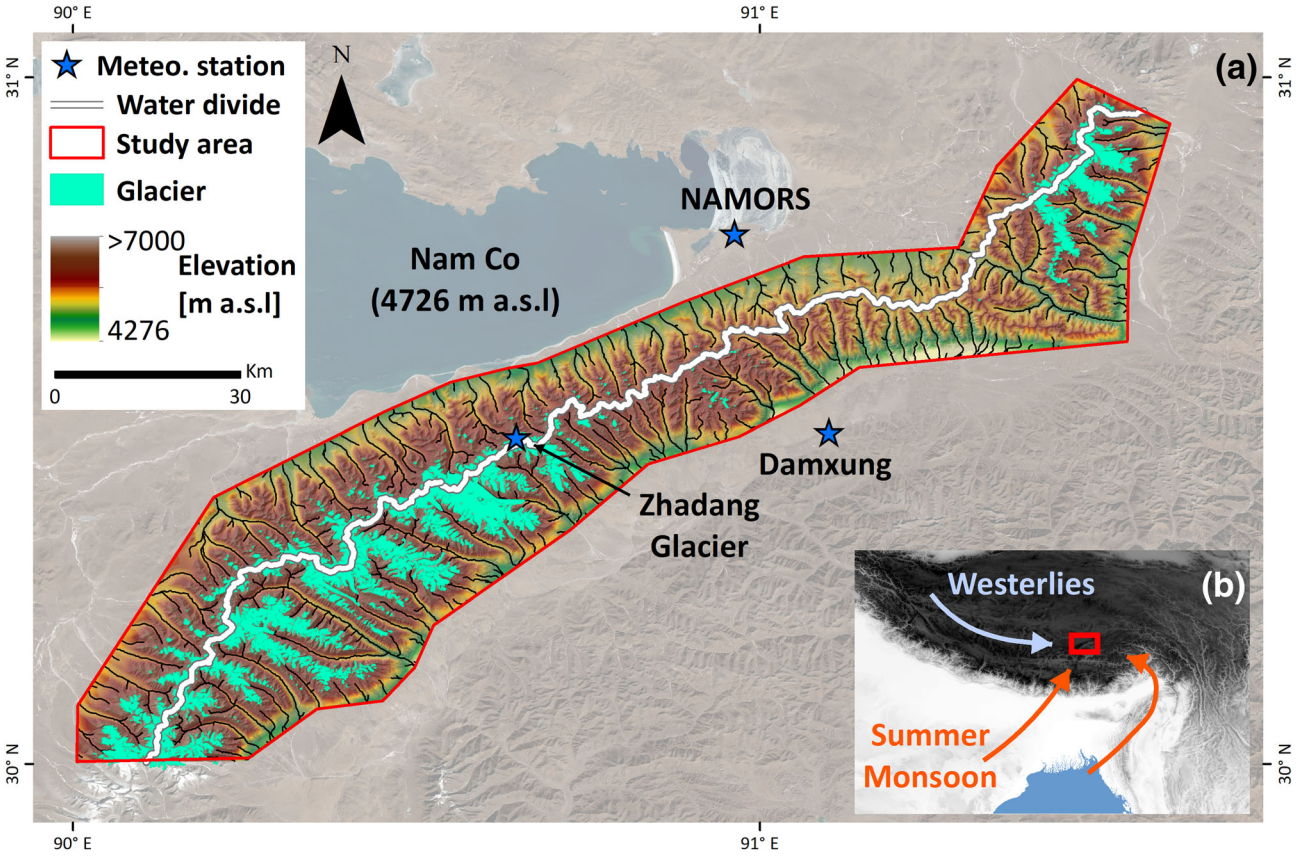

FIGURE 1 (a) Overview of the study area within the western Nyainqêntanglha Range and the location on the Tibetan Plateau. We display glacier outlines and background optical imagery based on Sentinel-2 data of January 30, 2018 (©Copernicus Sentinel data 2018, processed by ESA) and the geoid elevation of the TanDEM-X (©DLR, 2017; geoid heights of EGM96). (b) Major atmospheric systems affecting the study area in summer (Indian Monsoon) and winter (Westerlies) above the SRTM v4 elevation of the Tibetan Plateau[49,50] [Colour figure can be viewed at wileyonlinelibrary.com]

in a global rock glacier inventory. We use Sentinel-1 satellite data of 2016–2019 processed with InSAR time series techniques to estimate the interannual surface velocity and infer rock glacier activity. In the following we introduce our study area and related work of previous studies. We then explain the data and methods we used to generate the inventory. Finally we present the inventory followed by a discussion on the limitations of our methods, potential implications regarding the regional climate, and finally our conclusions.

2 | STUDY AREA: THE WESTERN NYAINQÊNTANGLHA RANGE

2.1 | Climate

The western Nyainqêntanglha Range is located in the southeastern center of the TP (Figure 1) with an elevation of ~4,500–7,162 m. The median elevation of the study area is 5,369 m with an interquartile range of 5,109–5,632 m. The study area is about 230 km in length

and covers an area of 4,622 km^2. The mountain range strikes from the southwest to the northeast, forming a climatic divide as a topographic barrier. Glaciers cover the highest parts and most other areas are considered to be in the periglacial zone.[51] The northern side of the mountain range drains mainly into the endorheic Nam Co, currently the second largest lake on the central TP with a surface area of 2,018 km^2.[52] Catchments on the southeastern side drain into the Yangbajain–Damxung Valley as part of the Tsangpo–Brahmaputra River system. The climate is controlled by the Indian Monsoon system in the south and the dry continental climate of Central Asia from the northwest (Figure 1b).[49] The Indian Monsoon delivers the majority of the annual precipitation within the summer period from June to September, while the Westerlies bring dry continental air and semi-arid conditions during the winter months.[53] Annual precipitation is higher on the southern side of the mountain range with 460 mm in Damxung from 1971 to 2000 compared to 406 mm at Nam Co Monitoring and Research Station for Multisphere Interactions (NAMORS) from 2006 to 2017 (Figure 2).[54,55] A meteorological station at Zhadang Glacier recorded an annual precipitation between 487 and 568 mm from 2009 to 2011.[56] The mean annual air temperatures at those meteorological stations during the same time periods were 1.6, −0.6, and −5.9°C respectively.

2.2 | Glaciers and lakes

The effects of climate change on glaciers and glacial lakes in the western Nyainqêntanglha Range and the TP as a whole are well documented. Large-scale remote sensing studies show that glaciers lost 22% of their surface area from 1977 to 2010[57] with a glacier mass balance of −0.3 m/yr from 2000 to 2017.[58] Most other regions on the TP show similar negative glacier mass balances with the exception of the northern TP, where positive mass balances are documented for some regions.[59] Multiple studies have investigated the changes to the extent of the Nam Co over the past decades, reporting an average increase of lake surface area of 0.1% per year since the 1970s.[52,60] The contribution of increased glacial meltwater to the increase in lake level was estimated to be 10% from 1971 to 2004 and 30% from 1990 to 2010 for different parts of the mountain range.[61,62] Glacial lakes have also been expanding greatly both in number and in surface area. Increases in the surface area of glacial lakes from 2.69 to 7.15 km^2 between 1972 and 2009 and 6.75 to 9.12 km^2 between 1976 and 2018 have been reported for different parts of our study area.[57,63]

2.3 | Permafrost and periglacial landforms

The study of permafrost and associated periglacial landforms in the western Nyainqêntanglha Range has received much less attention compared to glaciers and lakes.[55] InSAR time series analysis display seasonal heave–thaw cycles with an amplitude of up to 2.5 cm near water bodies.[64,65] Large-scale permafrost maps of the TP predict permafrost for most nonglaciated parts of the mountain range.[66,67] Field studies estimate a lower permafrost limit of 5,300–5,450 m in two north-oriented catchments.[68,69] They identified a small number of rock glaciers displaying moderate velocities of 5–10 cm/yr.[69] Rock glacier inventories on the TP are rare, though one recently identified 295 rock glaciers in Daxue Shan, southeastern TP.[13] Our study is the first to provide a rock glacier inventory of the western Nyainqêntanglha Range.

3 | DATA AND METHODS

Our general workflow to create the rock glacier inventory contains the following steps (Figure 3). First we generate the line-of-sight (LOS) surface velocity estimation from Sentinel-1 InSAR data and project it along the direction of the steepest slope (Sections 3.1 to 3.3). Then we create the manual rock glacier outlines based on optical satellite imagery, surface elevation data, and surface velocity (Section 3.4). A subset of the manually created rock glacier outlines is used to train the maximum-likelihood algorithm. A different subset acts as validation to identify the best feature selection for the

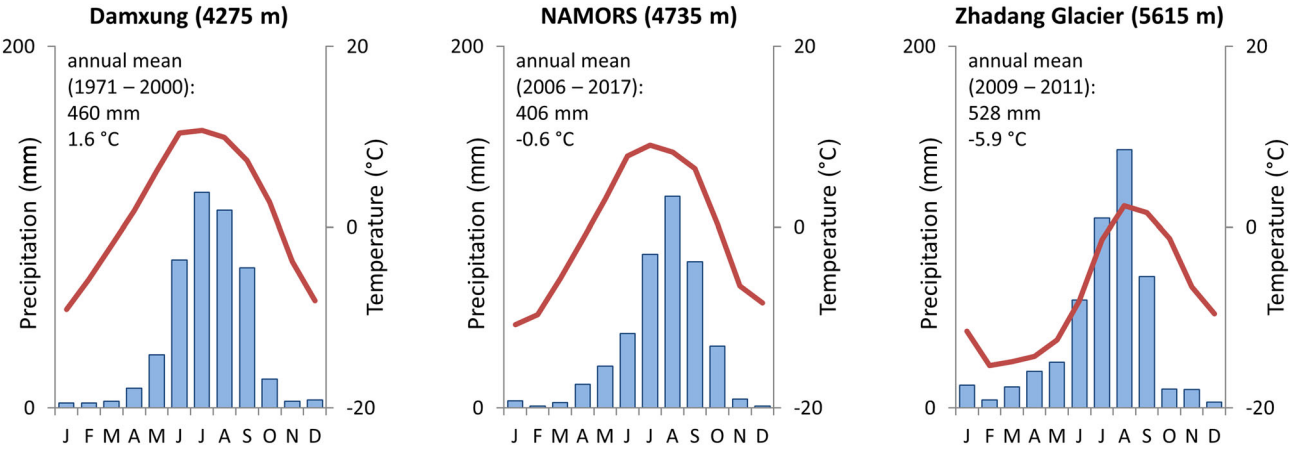

FIGURE 2 Meteorological data of three stations at the study area. Their locations are shown in Fig. 1[54–56] [Colour figure can be viewed at wileyonlinelibrary.com]

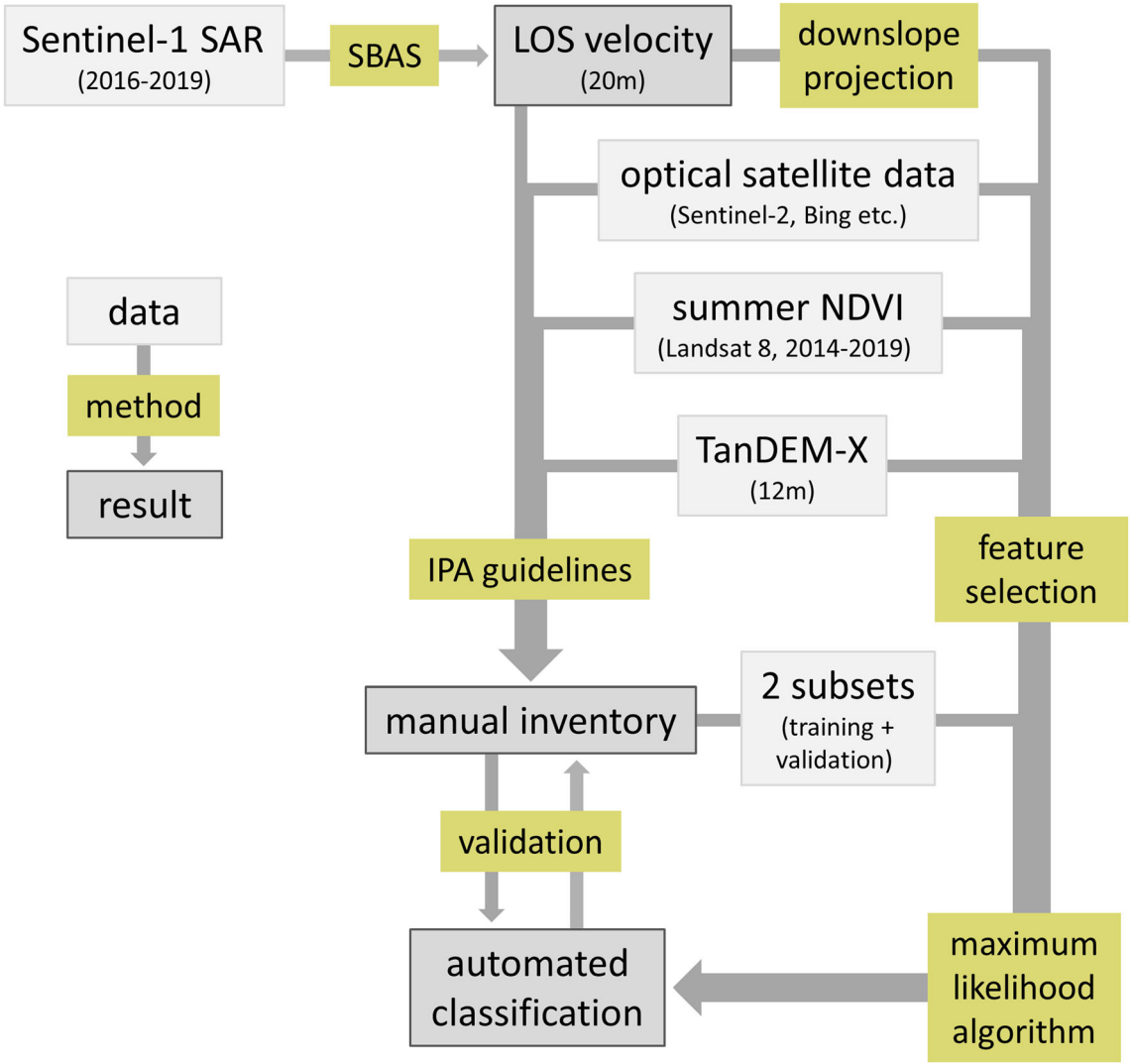

FIGURE 3 The workflow we followed to generate the manual rock glacier inventory and the automated classification results [Colour figure can be viewed at wileyonlinelibrary.com]

automated classification. Finally we create the automated classification results based on the resulting optimal feature selection and validate it against the entire manually created inventory (Section 3.5).

3.1 | InSAR processing

Interferograms are a spatial representation of the phase difference between two SAR acquisitions and can be used to determine LOS surface displacement.[37] The phase stability, so-called coherence, is often used to represent the quality of an interferogram. A variety of different InSAR algorithms are available to process consecutive interferograms to study surface displacement over several years, often referred to as InSAR time series analysis. InSAR time series analysis generally increases the accuracy of surface displacement estimations, as temporally uncorrelated atmospheric effects can be removed with filters.[70] Most studies employing InSAR techniques to investigate rock glacier velocity use individual SAR pairs (DInSAR) or relatively short time series analysis during the snow-free months.[7,35,45,47] Other related approaches include pixel tracking of optical or SAR images, though these are generally only used for fast-moving rock glaciers or for long temporal gaps between data acquisitions.[16,18] The winters in our study area are semi-arid, due to the dominance of the midlatitude westerlies during those months.[49] Our field work has shown that snow storms may occur in autumn, which causes decorrelation of InSAR data. The dry winter climate leads to stable backscatter properties of the frozen ground, which is reflected by good coherence values. We therefore opted to use a modified version of the Small Baseline Subset (SBAS) method,[71] which we performed with the ENVI SARScape software (©Sarmap SA, 2001–2020). The original SBAS method requires a pixel to be coherent in all interferograms during the observation period. The results often show large data gaps in seasonally variable areas where the coherence may not be high enough all the time due to changing backscatter properties. The SBAS algorithm we employ was originally described as "´intermittent SBAS"[72] and is included in SARScape as an option of the SBAS processing

chain labeled "disconnected blocks". Intermittent SBAS interpolates time periods where the coherence of a pixel drops below the chosen coherence threshold in some interferograms. This may occur due to heavy rainfall, snow cover, or large displacement. Intermittent SBAS results in a greatly improved spatial coverage compared to the original SBAS algorithm for partially vegetated study areas.[72,73] In our study area it helps to interpolate time periods in spring and autumn when the transition between snow-free summers and frozen ground in winter causes decorrelation. For our analysis we chose a coherence threshold of 0.2, which is lower than the threshold of 0.3 used by others for intermittent SBAS methods.[72,73] The lower threshold is justified in our opinion, as good spatial coverage is most important for this study. Pixels need to exceed the coherence threshold in at least 60% of all interferograms during our 3-yr observation period. A pixel may therefore contain up to 40% interpolated information, though the median value of all pixels on rock glaciers is only 2%.

We use Sentinel-1 Level-1 single look complex data from the interferometric wide swath mode to perform our InSAR time series analysis. The wide swath mode has a ground resolution of 20 m in azimuth and 5 m in range.[74] We used a multilooking factor of 4 in range and 1 in azimuth to achieve a ground resolution of 20 m. Sentinel-1 has been acquiring data since October 2014 but we only use data acquisitions from September 2016 to October 2019 due to temporal data gaps. Long temporal baselines of 48–96 days lead to strong underestimation of rock glacier velocity and poor coherence with earlier acquisitions. Sentinel-1 emits at a wavelength of ~5.6 cm.[75] Displacements larger than half the emitted wavelength between two acquisitions are likely to be underestimated during interferogram generation.[37] A temporal baseline of 96 days would result in a maximum detectable velocity of 10.6 cm/yr in LOS. It would therefore make the distinction between active and transitional rock glaciers very difficult. Sentinel-1 acquisitions of 2016 are available at 24-day intervals and at 12-day intervals from 2017 onwards. We use 80 acquisitions in ascending and 74 in descending geometry. The longest temporal data gap occurs in summer 2017. For the descending data set this causes a maximum temporal baseline of 72 days between two acquisitions during that time. There is no data gap in the ascending data set from September 2016 onwards. We chose a maximum temporal baseline of 60 days for ascending acquisitions. This results in a maximum detectable velocity of 17.0 cm/yr in ascending geometry and 14.2 cm/yr in descending geometry. The velocity of faster landforms can therefore not be determined reliably though it can still be detected very well. We generated a total of 181 interferograms in ascending geometry and 163 in descending geometry for the 3-yr observation period. The time–position plots for both the ascending and the descending time series are included in the Supporting Information. Some parts of the study area show coherence values below our chosen threshold of 0.2, especially in the northeastern part in the descending geometry. We therefore selected a temporal subset of 14 interferograms for ascending and 13 interferograms for descending geometry from October 2017 to February 2018. This time period displays good coherence values throughout the study area and we used the SBAS results of this shorter period to fill in spatial data gaps in our 3-yr time series results.

3.2 | Removal of large-scale phase delay

It is necessary to carefully select stable reference points in the study area to achieve InSAR results with a high accuracy.[37] Poorly selected reference points can introduce seasonal artifacts and interannual shifts leading to misinterpretation of displacement patterns. No long-term data from the global navigation satellite system is available for this area to act as reference points. We therefore selected probable stable areas on the outskirts of the mountain range for our reference points. These 385 reference points were placed along both the northern and the southern side of the mountain range. We only selected points without visible signs of displacement and with high coherence throughout all interferograms. We avoided areas near the valley bottom during the selection of our reference points, as they probably experience heaving and thawing related to freezing and thawing of the ground.[64,65] We applied an atmospheric high pass filter of 100 days and a low pass filter of 1,200 m to reduce atmospheric artefacts.

3.3 | Downslope projection

We projected the LOS surface velocity of both geometries in the direction of the steepest slope.[75] The following areas were masked prior to the projection: (a) areas of glaciers where free ice is visible; (b) areas with a slope <2°, as these areas are generally too flat to support downslope motion[76]; and (c) areas with a low slope and strong vertical displacement signal (based on a decomposition of ascending and descending time series results). This displacement is probably not gravity-driven and therefore not directed along the steepest slope. (d) We masked wetlands and the immediate surrounding of rivers and lakes. Changing soil moisture in these areas may lead to a false identification of displacement.[77]

To perform the downslope projection, we calculated a sensitivity coefficient with a value between 0.2 and 1 and divided the LOS velocity by this coefficient to receive the downslope velocity. A sensitivity coefficient of 1 represents slopes where the angle between the LOS vector and the downslope direction is zero. The sensitivity of the satellite to displacement in that direction is therefore very high. A sensitivity coefficient of 0.2 represents areas where the angle between the LOS vector and the downslope direction is large. The sensitivity of the satellite to displacement in that direction is therefore very small. Ascending and descending data sets have different LOS and their respective sensitivity coefficients are therefore also different when observing the same area. We included the spatial distribution of this sensitivity coefficient in the Supporting Information. After projecting both ascending and descending data sets into the downslope direction, we combined both data sets according to the following criteria:

1. We only use the downslope projection of the more sensitive geometry in areas where the sensitivity coefficient of the more sensitive geometry is at least 50% larger than the sensitivity coefficient of the other geometry and is larger than 0.2.

2. We calculate the mean value of the downslope projections of both geometries in all other areas, as the sensitivity of neither geometry is clearly superior.

When we refer to the velocity in the text hereafter, we are referring to the combined downslope velocity of both ascending and descending geometries. The only exception is where we specifically refer to the LOS velocity.

3.4 | Optical satellite and DEM products

We use seven optical Landsat 8 acquisitions with a 30-m resolution to calculate the summer Normalized Difference Vegetation Index (NDVI) in our study area. The NDVI is calculated from the red and near-infrared bands (bands 3 and 4 for Landsat 8) and is a measure of vegetation density and productivity. Moving rock glaciers are generally sparsely vegetated and have lower NDVI values than their immediate surrounding, potentially making NDVI a valuable indicator to identify rock glaciers.[40,78] Combining multiple acquisitions is necessary due to the partial or full cloud cover associated with the summer monsoon climate in the study area. The Landsat 8 data sets were acquired on the following dates: August 12, 2014, July 30, 2015, May 16, 2017, June 1, 2017, June 20, 2018, July 25, 2019 and August 26, 2019. We chose these dates, as they represent the Landsat 8 acquisitions with the lowest cloud cover during the growing season of May to September.[79] The irregularity of these dates may introduce a bias but they were necessary to produce an NDVI map with near total coverage of the study area. We masked snow-covered areas as well as clouds and their shadows prior to the calculation of the NDVI. The NDVI data sets were then merged into one raster with pixels present in multiple NDVI data sets receiving their mean value. The free ice glacier outlines were derived from a cloud-free Sentinel-2 acquisition of January 30, 2018 with a supervised maximum-likelihood classification and checked manually.

We use the 12-m-resolution TanDEM-X (©DLR, 2017) Digital Elevation Model (DEM) to perform all topographic analysis and to remove the topographic phase from the InSAR data. This global DEM was acquired between 2010 and 2015 using single-pass X-Band SAR interferometry and released by the German Aerospace Agency in 2017.[80] In our study area it has a vertical accuracy with an interquartile range of 0.26–0.40 m in areas with a slope <40° and 0.77–1.83 m in steeper areas.

3.5 | Manually generating the rock glacier inventory

We followed the guidelines of the IPA Action Group on "Rock glacier inventories and kinematics" to identify, outline, and classify all actively moving rock glaciers in the study area.[38] These guidelines consist of two detailed documents describing the baseline concepts and practical guidelines of which we used versions 4.1 and 3.0.1 respectively.[39] The guidelines propose a general methodological framework for inventorying rock glaciers using InSAR. They recommend generating point information to identify individual rock glacier units and outlines to locate the moving part of the rock glacier. Our first step was therefore to identify rock glacier units based on the interpretation of surface velocity, optical satellite imagery, and DEM data. The initial point identification was performed by one analyst and then checked and adjusted by two other experts. After this initial step the outlines were generated manually and checked and adjusted again by two experts.

The following data sets were used for the identification and outlining process: (a) optical imagery from Bing Maps, Google Earth, Zoom Earth, and a cloudless and largely snow-free 10-m-resolution Sentinel-2 acquisition of January 30, 2018; (b) hillshade and slope maps derived from the 12-m-resolution TanDEM-X DEM and (c) NDVI derived from seven Landsat 8 summer acquisitions; and (d) median surface velocity from 2016 to 2019 based on Sentinel-1 data. Mandatory criteria of a rock glacier in our study are clearly discernible frontal and lateral margins overriding the surrounding terrain. In some instances, optical and DEM data may suggest different outlines due to georeferencing errors. The rock glacier outlines were drawn to match the DEM data in those cases, as we consider it to be more reliable. Optional criteria are a ridge-and-furrow topography associated with compressive flow and a reduced NDVI compared to the surrounding, indicating a lack of vegetation due to active creeping. Rock glaciers are classified as transitional or active according to their surface velocity. Rock glaciers without a clear surface velocity are only included if the sensitivity of InSAR is low in this area, in which case they are included with an undefined activity. Debris-covered glaciers and rock glaciers represent two ends of a continuum.[3,10] Debris-covered glaciers with visible bodies of ice upslope are not included in the rock glacier inventory.

We decided to add an additional attribute not included in the IPA guidelines to the rock glacier outlines, to describe the morphology of the rock glacier in greater detail (Figure 4). This attribute is important for further investigations regarding the evolution of rock glaciers in the mountain range. Here, we differentiate between debris rock glaciers (morainic origin) and talus rock glaciers (rock wall origin).[1] For talus rock glaciers we adopted the definitions of detailed studies,[81,82] as these fit well to the morphology of rock glaciers we observe in the western Nyainqêntanglha Range. Protalus lobes and protalus ramparts are underlying landforms of debris mantles, scree slopes, or rock walls.

3.6 | Supervised maximum-likelihood classification

Manually outlining rock glaciers is inherently subjective and dependent on the experience of the analyst. Multiple studies in recent years have therefore evaluated different classification algorithms and varying input parameters to automatically identify and classify rock glaciers.[40–44] In addition to the manual approach described above, we also performed a pixel-based supervised maximum-likelihood

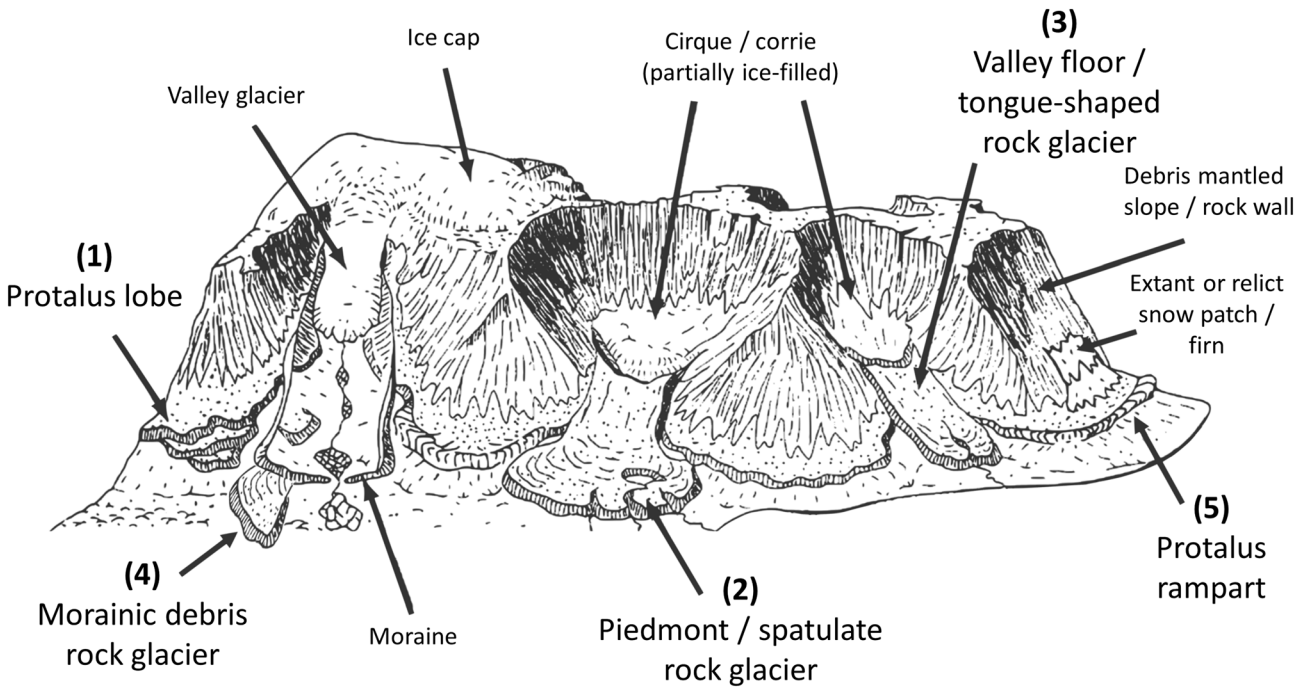

FIGURE 4 Schematic view on rock glacier morphology and protalus ramparts of the western Nyainqêntanglha Range. Numbers in parentheses refer to the different morphological classes of rock glaciers (found in the inventory as the attribute "morph_clas").changed after the literature.[81,82] Examples of the different morphological classes in the study area are included in the Supporting Information

classification. We masked glaciers, flat areas, wetlands, and the immediate surrounding of rivers and lakes (see section 4.3). We used the ENVI software to perform the automated classification based on the surface features described in Table 2. The input parameters (such as elevation, slope, or NDVI) which the classification algorithm uses to identify rock glaciers, are referred to as features hereafter. Our initial feature selection comprises features which were successfully used by similar studies to identify rock glaciers.[40–42]

First, we identified the most suitable feature combination to automatically classify rock glaciers in the study area. We selected 40 rock glaciers with clear outlines spread throughout the study area to validate and adjust the performance of different feature combinations. Of those rock glaciers, 25 were randomly chosen as training areas, while the remaining 15 rock glaciers were used to validate the performance. We also selected 20 nonrock glacier areas, to assess the number of pixels falsely classified as rock glacier. We evaluated different feature combinations to determine the most suitable selection to automatically classify rock glaciers in our study area. All features were resampled to the 12 × 12-m resolution of the TanDEM-X DEM. For the initial evaluation we performed the classification with the following five features: elevation, slope, NDVI, slope variability, and height error. Elevation, slope, and NDVI scored highly in a similar study by Brenning et al.[40] Slope variability was to represent surface roughness. Height error was included to avoid false classifications of slopes with high noise levels due to the associated high surface roughness. To validate the importance of each of the five initial features, we then repeated the classification with just four of the initial five features (leaving out a different feature every time). All classifications with only four of the five initial features performed worse. This confirmed the importance of all five initial features. We then performed the classification again with the five initial features and different combinations of the remaining features to determine the optimal feature combination.

4 | RESULTS

4.1 | Accuracy of surface velocity

It was not possible to validate the results of our time series analysis with other data sets such as terrestrial measurements as no such data were available to this study. To evaluate the reliability of our data, we therefore analyzed the surface displacement calculated by the time series analysis in areas that were probably stable during the observation period. We analyzed all areas with a slope <5° that are not part of a clearly subsiding structure or are in the vicinity (<200 m) of a stream, lake, or wetland. The interquartile range of all pixels ($n = 194{,}114$) in probable stable areas in LOS is −0.3 to 0.6 cm/yr on the northern side of the mountain range in ascending geometry and −0.6 to 0.2 cm/yr in descending geometry. On the southern side ($n = 67{,}230$) the interquartile range is −0.8 to −0.1 cm/yr in both geometries. The median coherence on rock glaciers is 0.33 with an interquartile range of 0.27–0.41.

TABLE 2 Description of all surface features evaluated for automated rock glacier classification

Feature	Description	Resolution
Elevation	The elevation displayed by the TanDEM-X DEM	12 m
Slope	The slope derived from the TanDEM-X DEM	12 m
Surface velocity	The downslope velocity is based on Sentinel-1 SAR data of 2016 to 2019	20 m
Sentinel-2	Bands 2 and 3 of Sentinel-2 from January 30, 2018. These correspond to central wavelengths of 490 nm (blue light) and 560 nm (green light), respectively[83]	10 m
Height error	Auxiliary data set displaying the vertical accuracy of the TanDEM-X DEM	12 m
North exposure/east exposure	These features are derived from a pixel's aspect, describing how close a pixel's aspect is to north exposure or east exposure	12 m
Slope variability	Slope variability is a measure of surface roughness and represents the variation in slope within the 8 surrounding pixels[84]	12 m
NDVI	Summer NDVI of seven Landsat 8 acquisitions of 2014 to 2019	30 m
Topographic position index (TPI)	The TPI displays the elevation of a pixel relative to the mean elevation of its surrounding.[85] Different landforms can be highlighted by choosing different search radii around the pixel to calculate the mean elevation. We evaluate the impact of the TPI with a radius of 200 m and with a radius of 800 m	12 m

4.2 | Manual rock glacier inventory

The rock glacier inventory contains a total of 1,433 rock glaciers (Table 3; Figure 5). The IPA guidelines classify rock glaciers with a maximum velocity of 1–10 cm/yr as transitional, and faster rock glaciers as active. If the velocity of a rock glacier was very close to the higher activity class we assigned it the higher class. Relict rock glaciers with velocities below 1 cm/yr are not part of this inventory. We included rock glaciers without clear surface velocity signal, if their probable motion direction is one that InSAR is not sensitive to (i.e., north or south). These rock glaciers and other rock glaciers in areas with poor InSAR sensitivity are classified as "undefined" regarding their activity. Undefined rock glaciers represent 15.6% of the inventory; 65.9% are transitional and 18.5% are active. Rock glaciers cover a combined area of 124.9 km^2 equivalent to 2.7% of the study area. Free ice glaciers cover a combined area of 575.7 km^2. The water divide splits the study area into a northern and a southern side. The northern side has a median elevation of 5,319 m, represents 41% of the study area, 26.0% of the free ice glacial area and contains 20.9% of all rock glaciers. The southern side has a median elevation of 5,411 m, and represents 59% of the study area, 74.0% of the free ice glacial area, and 79.1% of all rock glaciers. In total, 91.3% of all active rock glaciers are located south of the water divide. Rock glaciers on the southern side are located at lower elevations (median = 5,321 m) compared to the northern side (median = 5,408 m). The lowest rock glacier reaches an elevation of 4,498 m, while the highest reaches 5,899 m. A summary of this data can be found in Table 3.

Protalus lobes are the most common morphological class, representing 67.4% of all rock glaciers and 51.6% of the total rock glacier area (Figure 6). Spatulate and tongue-shaped rock glaciers include the largest rock glaciers. Together they represent 13.3% of all rock glaciers and 29.4% of the rock glacier area. Morainic debris rock glaciers are distributed at the highest altitude with a median elevation of 5,478 m. Protalus lobes and protalus ramparts display the lowest velocity with only 11.5% of the former and none of the latter being active. Of the 24 spatulate rock glaciers 12 (50%) are active and of the 166 tongue-shaped rock glaciers 65 (39.2%) are active. Spatulate rock glaciers are only present south of the water divide.

TABLE 3 Summary of spatial information of the rock glacier inventory. Elevation takes into account all pixels within rock glaciers of either the northern or the southern side. Range refers to the difference in elevation between the highest and lowest pixel in a rock glacier

	North (300 rock glaciers)			South (1,133 rock glaciers)		
	Median	Interquartile range	Range	Median	Interquartile range	Range
Elevation (m)	5,408	5,319–5,505	4,943–5,827	5,321	5,200–5,442	4,498–5,899
Range (m)	81	59–117	19–311	104	72–156	14–584
Surface area (ha)	5.0	3.0–9.2	0.5–102.9	5.1	2.6–10.5	0.3–102.1

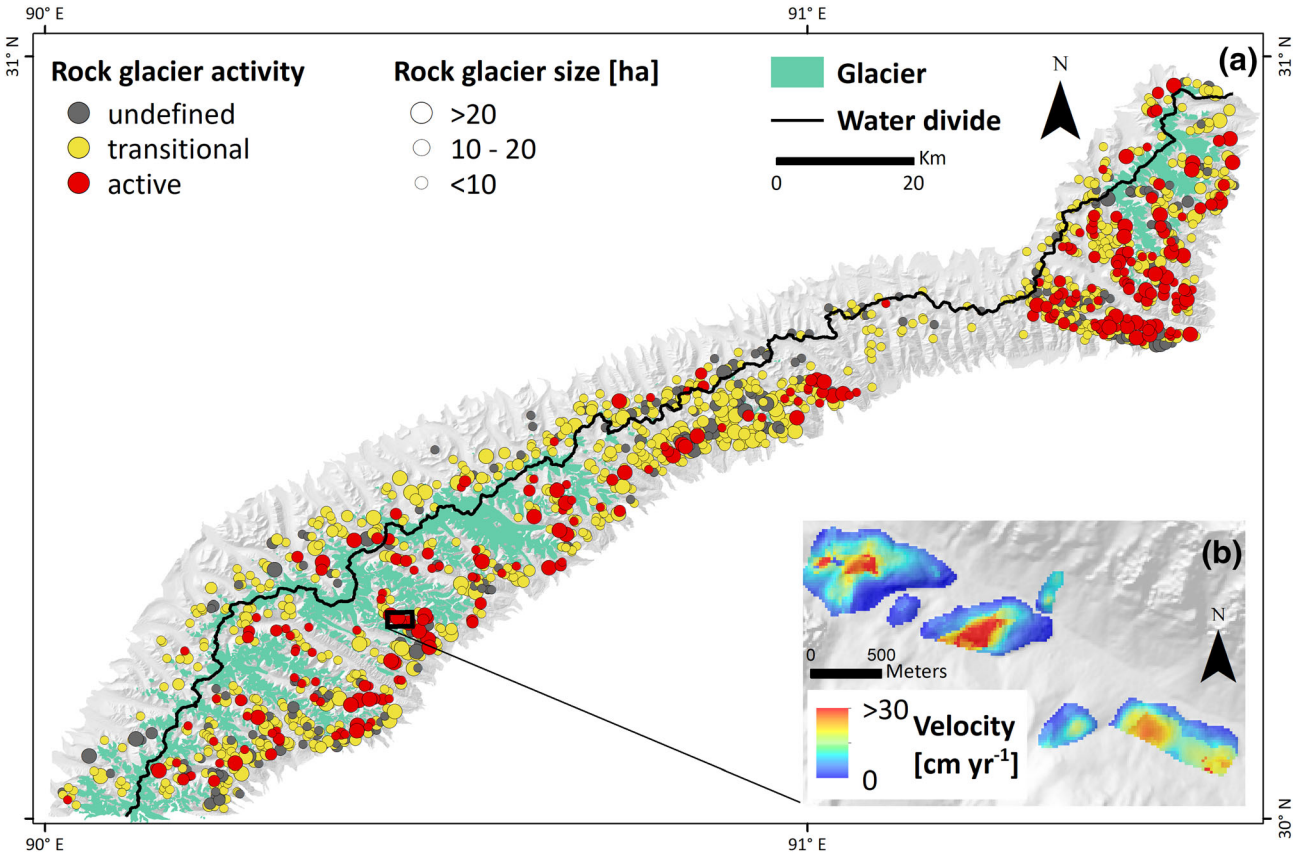

FIGURE 5 Overview of the manually determined rock glacier inventory. (a) All rock glaciers mapped in the study area. Rock glacier activity is based on their median surface velocity of 2016 to 2019. The activity classification follows the IPA guidelines. Rock glaciers with a surface velocity of 1–10 cm/yr are considered transitional and faster rock glaciers are considered active. (b) A valley with active rock glaciers and their downslope velocity in greater detail (©Copernicus Sentinel data 2016–2019, processed by ESA; ©DLR, 2017) [Colour figure can be viewed at wileyonlinelibrary.com]

4.3 | Maximum-likelihood estimation

The best result was achieved by combining the following nine features: downslope velocity, elevation, slope, NDVI, slope variability, height error, TPI with 200 m radius, and Sentinel-2 bands 2 and 3. We give an overview of these features in Table 2. In total, 84.0% of the pixels in the 15 validation rock glaciers were correctly classified with this combination. In total, 3.2% of the pixels in the 20 nonrock glacier areas were falsely classified as rock glaciers. The true positive rate is therefore 84.0% and the false positive rate is 3.2% for our validation areas.

After identifying the most suitable features for the classification, we evaluated the performance of the automated classification compared to the entire manually created rock glacier inventory. We use three metrics to evaluate the performance: true positive rate (TP), false positive rate (FP) and object identification (OI). TP describes the percentage of pixels within the manual rock glacier outlines, which were correctly classified as rock glacier. FP refers to the percentage of pixels outside the manual outlines, which were falsely classified as rock glacier. OI describes the percentage of manual outlines with a TP of at least 30.0%. In total, 87.8% of all rock glaciers were correctly identified by the OI (Table 4). Smaller rock glaciers are less likely to be identified. In total, 85.9% of rock glaciers smaller than 10 ha were identified, compared to 96.5% for rock glaciers larger than 20 ha. In total, 97.3% of active rock glaciers, 85.1% of transitional rock glaciers, and 87.8% of rock glaciers with undefined activity were identified. The entire inventory displays a TP of 69.5% and an FP of 10.4% (example area in Figure 7). In total, the automated classification predicts a combined rock glacier area of 428.4 km^2. This is equivalent to an overestimation of 243.0% when compared to the 124.9 km^2 of manually outlined rock glaciers. After checking the manual outlines against the automatic classification, we identified 18 additional rock glaciers. To assess the relative importance of the features to each other, we repeated the classification with only eight of the nine features (leaving out a different feature every time). The resulting feature ranking is presented in Table 5.

5 | DISCUSSION

5.1 | InSAR limitations

While InSAR time series techniques have great potential to monitor slow surface velocity over time, they are not without considerable

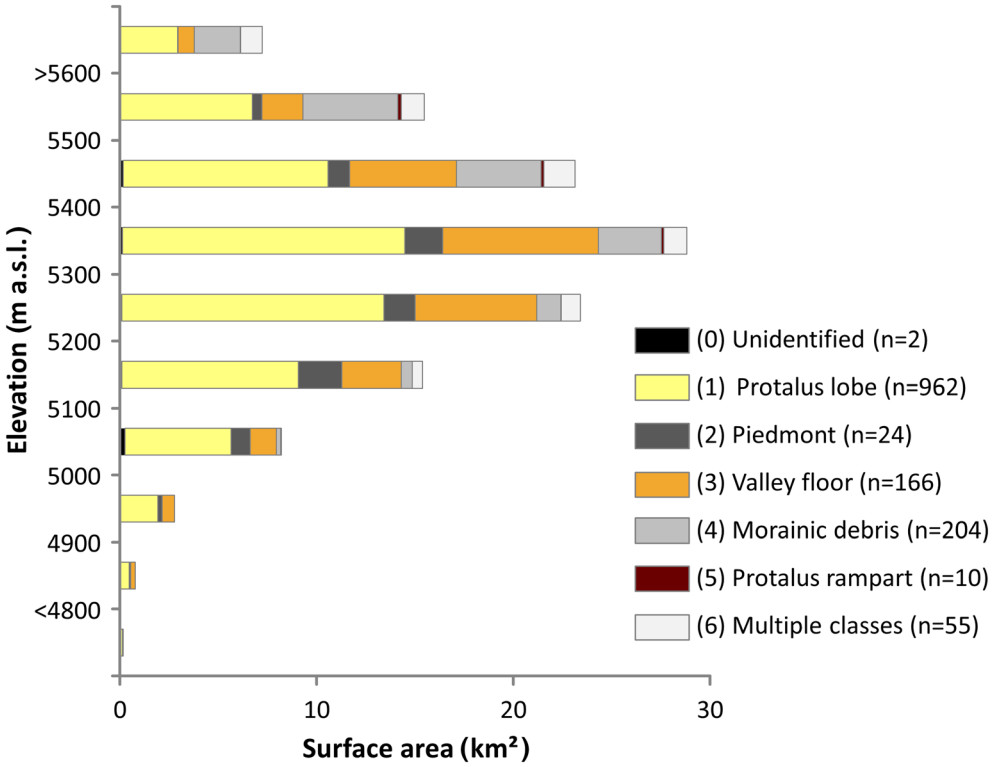

FIGURE 6 Elevation distribution of rock glacier area divided into their respective morphological classes. Numbers in parentheses refer to the different classes of rock glaciers (found in the inventory as the attribute "morph_clas") [Colour figure can be viewed at wileyonlinelibrary.com]

TABLE 4 True positive rate (TP) and object identification (OI) of the automated classification for different size and activity classes

Rock glacier classes		TP (%)	OI (%)
Entire inventory		69.5	87.8
Surface area	<10 ha	66.5	85.9
	10–20 ha	70.0	91.6
	>20 ha	69.3	96.5
Activity	Active	75.3	97.3
	Transitional	63.1	85.1
	Undefined	69.9	87.8

limitations. These limitations include the low sensitivity towards displacement with a strong north or south component, the maximum detectable displacement between two SAR acquisitions, decorrelation due to changing surface properties and the influence of atmospheric delay.

The issue of InSAR sensitivity is well known and causes issues especially for landforms with very low displacements. Projecting the LOS displacement into the assumed direction of motion (i.e., along the steepest slope) does produce more representative results[75] but their velocities are probably still underestimated to some extent. Rock glaciers in areas with poor InSAR sensitivity are included in the inventory even if their LOS velocity is <1 cm/yr for that reason. Their activity is classified as "undefined." Other rock glaciers with slightly higher LOS velocity but also located in areas where InSAR sensitivity is poor received the same classification. A map displaying the approximate InSAR sensitivity to downslope motion for each pixel is included in the Supporting Information.

The maximum detectable displacement between two SAR acquisitions is equal to half the wavelength of the emitting satellite (i.e., ~2.8 cm for Sentinel-1). Larger displacements cannot be unwrapped reliably and even displacements greater than a quarter of the wavelength, or 1.4 cm for Sentinel-1, may lead to aliasing effects.[37] Most of the interferograms used for our analysis have temporal baselines of either 12 or 24 days but a small number have much larger baselines of up to 72 days. This is due to temporal data gaps of the descending Sentinel-1 data set in summer 2017. The maximum detectable LOS velocity is 17.0 cm/yr in ascending geometry and 14.2 cm/yr in descending geometry. An underestimation of the velocity due to aliasing effects may occur where the LOS velocities exceed 8.5 cm/yr in ascending geometry and 7.1 cm/yr in descending geometry. Most transitional rock glaciers display LOS velocities below these thresholds but the velocity of active rock glaciers is probably underestimated in this study. Rock glaciers with a maximum LOS velocity very close to 10 cm/yr were therefore classified as active to compensate for this underestimation.

Vegetation growth, snow fall, and soil moisture variations between two SAR acquisitions may cause decorrelation or misinterpretation of InSAR data.[16,72,73,77] The high altitude of our study area means that large vegetation, such as trees, are not a problem. Actively moving rock glaciers are sparsely vegetated, and we therefore consider vegetation to have little impact on our InSAR results.[78] The winter climate in our study area is semi-arid.[53] Optical satellite imagery shows that snow fall occurs mainly between autumn and spring but our field work has shown that it may also occur in summer. We observe the lowest overall coherence during the spring and autumn months, which we attribute to the transition between frozen and

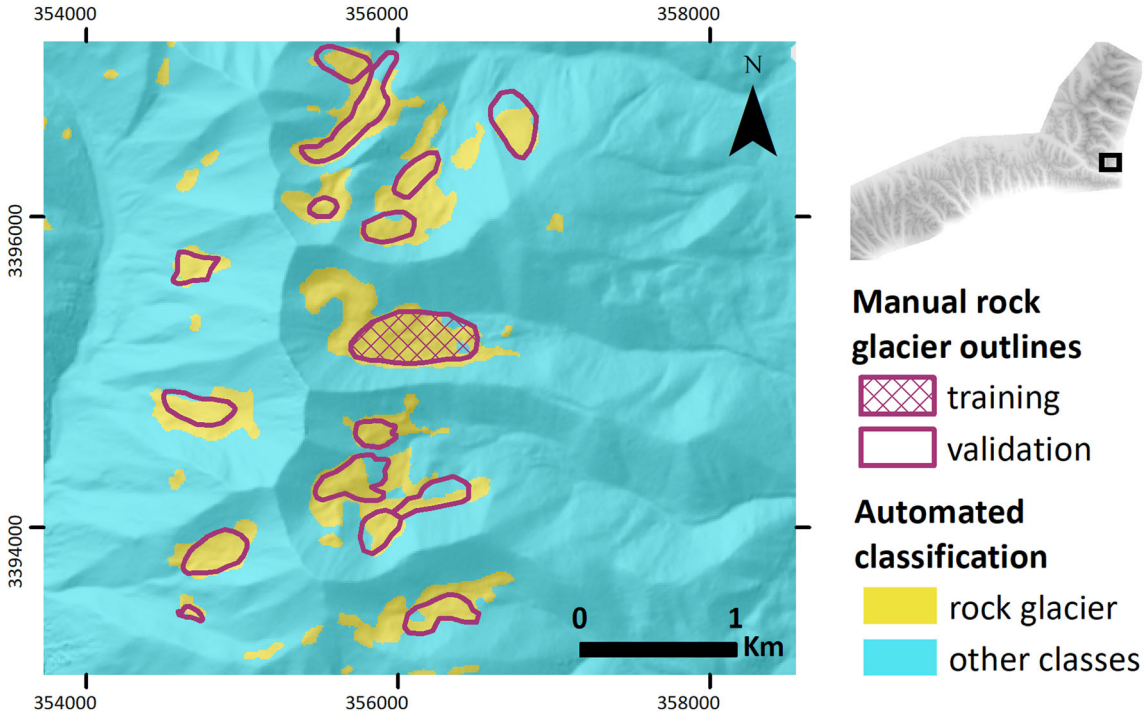

FIGURE 7 Example of the automated classification results compared to the manual rock glacier outlines. Yellow areas were classified as rock glacier and turquoise areas received other classes (e.g., debris slope, gully, ridge, etc.; ©Copernicus Sentinel data 2016–2019, processed by ESA; ©DLR TanDEM-X, 2017; Landsat-82,014–2019 courtesy of U.S. Geological Survey) [Colour figure can be viewed at wileyonlinelibrary.com]

TABLE 5 Feature ranking showing the change in true positive rate (TP), false positive rate (FP) and object identification (OI) if a feature is excluded from the classification process. The three features with highest impact in each column are shown in bold

Omitted feature	TP (%)	FP (%)	OI (%)
Downslope velocity	+1.9	+2.2	−0.9
TPI	**−12.6**	**−4.2**	**−9.8**
Slope variability	**−9.6**	−0.2	**−10.1**
Slope	**−6.6**	**−2.8**	−3.8
NDVI	−1.6	−0.1	−0.6
Height error	−4.6	−1.7	−4.3
Elevation	−3.5	**−2.3**	−1.3
Sentinel-2 Band 2	−4.4	−1.3	−3.8
Sentinel-2 Band 3	−5.9	−1.4	**−4.7**

unfrozen ground. The overall coherence is highest in winter, when the frozen ground leads to stable backscatter conditions. We chose a coherence threshold of 0.2 and employed the intermittent SBAS algorithm to perform temporal interpolation for pixels with lower coherence values in up to 40% of interferograms. These thresholds are lenient compared to most InSAR applications but they are necessary to achieve the aims of this study. We use the surface velocity to help with the manual identification of active rock glaciers and as a feature in the automated classification. We use only the median surface velocity from 2016 to 2019. The need for good spatial coverage therefore justifies the large amount of temporal interpolation in our opinion.

Varying types of atmospheric properties may delay the microwave emitted from the satellite, leading to major uncertainties in InSAR analysis.[86] The two dominant types we observe in our study area are turbulent delay and seasonal stratified delay. Turbulent delay is associated with short-term variations in the atmosphere and can be considered random in time. We observe the effect of turbulent delay in our individual interferograms, where they lead to false identification of surface displacement of up to half a phase cycle. As turbulent delay is random in time, its effect on longer observation periods becomes negligible. We therefore consider the effect of turbulent delay on our time series results to be relatively small. Seasonal stratified delay may lead to an apparent seasonal cycle in the surface displacement if there is a large elevation difference between the reference points and the area of interest.[87] This does not affect the interannual surface velocity and we therefore expect its effect to be negligible for this study.

5.2 | Rock glacier inventory

In this section we discuss the general characteristics of the rock glacier inventory and compare it to similar inventories of other studies. We also provide suggestions regarding the underlying climatic drivers. In total, 65.9% are classified as transitional with velocities of 1–10 cm/yr and 18.5% are considered active with velocities >10 cm/yr. Rock glaciers are more numerous and more active on the

southern side of the mountain range, which contains 91.3% of all active rock glaciers. The majority of the moisture available in this region is delivered by the Indian Monsoon from the south and southeast.[49] The southern (windward) side receives most of this moisture, which results in larger glaciers compared to the northern side.[54] It is likely that the higher moisture availability also facilitates the higher number and activity of rock glaciers.

Similar rock glacier inventories using comparable methods based around InSAR velocity have been published for the Swiss Alps, the dry Andes, the Sierra Nevada, and the Northern Tien Shan (Table 1). Rock glaciers velocities range from 2.2 to 170 cm/yr in the Andes and from 14 to 87 cm/yr in the Sierra Nevada.[7,47] The study in the Andes by Villarroel et al. used InSAR velocity only to detect active rock glaciers and does not quantify their individual velocities. Rock glacier velocities in the Tien Shan reach 114 cm/yr in China and 6.5 m/yr near the border between Kazakhstan and Kyrgyzstan.[18,45] We observe slower velocities for most rock glaciers in the western Nyainqêntanglha Range. This can be attributed to the limitations of different InSAR techniques used to estimate the velocity. The SBAS time series technique applied in this study is well suited to display the interannual velocity of transitional rock glaciers but underestimates the velocity of active rock glaciers (discussed in Section 5.1). These other studies use individual interferograms or short periods of consecutive interferograms to determine surface displacement. In individual interferograms, small displacements are often difficult to distinguish from short-term atmospheric signals. It is therefore likely that the displacement of some slow-moving rock glaciers could not be identified clearly, leading to an underrepresentation of slow-moving rock glaciers in these other studies. We use 74–80 consecutive acquisitions over a period of 3 years to calculate rock glacier velocity. This allows us to filter out temporally random atmospheric signals and also identify small displacements on slow-moving rock glaciers. Three of these other studies based their velocity estimations exclusively on summer acquisitions due to snow cover during spring and winter. Rock glaciers generally move faster during summer and autumn due to the increased temperature and moisture availaibility.[33–35] Deriving the annual velocity of a rock glacier solely from summer and autumn is therefore likely to lead to an overestimation. We include the often slower winter and spring seasons, leading to a lower interannual velocity of rock glaciers in our inventory. The probable velocity overestimation of these other studies combined with the underestimation of active rock glaciers in our study can therefore explain the difference in observed velocity.

5.3 | Semi-automatic classification

The classification algorithm used in this study is a supervised maximum-likelihood classification. Initial testing had shown that this algorithm performs better than other classification algorithms of the ENVI environment in our study area. We did not assess the performance of other classification algorithms outside the ENVI environment. ENVI is a popular remote sensing environment and easy to use without in-depth machine-learning knowledge. However, this also precludes the use of more sophisticated machine-learning algorithms. The algorithm used in this study performs the classification based on individual pixel values. Other algorithms, such as convoluted neural networks, take into account more complex patterns and textures.[42,43] These algorithms would probably perform better to separate rock glaciers from other debris-covered landforms, such as debris-covered glaciers.

The following features are used for the automated classification: downslope velocity, elevation, slope, height error, slope variability, terrain position index (TPI) with 200 m radius, NDVI, and Sentinel-2 bands 2 and 3. The TPI represents the elevation of a pixel relative to its surrounding. The search radius by which the surrounding is defined is determined by the analyst and therefore subjective. We performed the automated classification with different feature combinations including TPI with different search radii (200 and 800 m). The classification performed slightly better with a TPI of 200 m search radius. The true positive rate (TP) was 1.4% higher compared to using a TPI with radius 800 m. We therefore conclude that the impact of the subjectively chosen search radius is relatively small. TPI, height error, slope, and slope variability have the largest impact on the TP and object identification (OI). This partially agrees with similar studies that determined NDVI and slope to be most important in their study areas.[40,41] Elevation and NDVI were the most important features in the study of Kofler et al. evaluating different classification algorithms to differentiate between intact and relict rock.[44] NDVI is the least impactful feature in our classification. The high elevation of our study area prevents large vegetation from growing and our field work has shown that even smaller shrubs are rare. This leads to a low NDVI on the debris material surrounding the rock glacier and may explain why NDVI was not very impactful for this study. Excluding features from the automated classification leads to a lower false positive rate (FP) in some cases, especially in the case of TPI. These features are still worth including as they improve the OI metric, which we consider most important to generate a complete inventory.

Using InSAR surface velocity reduces FP from 12.6% to 10.4% but it also imposes the limitations associated with InSAR onto the automated classification. We discuss these limitations in detail in section 6.1 and will therefore focus here on the most important limitations: InSAR sensitivity and spatial data coverage. InSAR techniques have poor sensitivity towards displacement with a strong north or south component. Rock glaciers moving mainly into those directions are therefore probably excluded from the classification if their overall velocity is slow or if they are inactive. High spatial coverage of InSAR surface velocity data is necessary to apply our approach to a study area. This can be difficult to achieve in high mountain areas, where heavy snow fall may lead to decorrelation of InSAR in winter.[16] Using exclusively snow-free summer acquisitions or exploiting the low coherence associated with moving landforms could be an alternative in those regions.[88] Our automated classification approach is likely to work well in other regions with dry winter climates, such as the central and northern TP. Stable winter conditions in the northern Tien Shan make this region another potential candidate.[18]

The supervised maximum-likelihood classification produced a TP of 69.5% when compared with the entire manual rock glacier inventory. Rock glaciers >20 ha are identified with good accuracy (OI = 96.5%). Rock glaciers <5 ha are overlooked more frequently (OI = 85.9%). This is probably due to the large pixel size relative to the size of small rock glaciers. The recent study of Robson et al. correctly identified 108 of 120 rock glaciers with their automated detection approach in Chile and the Central Himalaya using Convoluted Neural Networks (CNNs) and object-based image analysis.[42] They also observed good results for large rock glaciers and less accurate predictions for small rock glaciers. They observed an increase from 62.9 to 72.0% in their TP by using optical satellite data with 2 m resolution instead of 10 m. The preliminary study of Marcer et al. used CNNs to identify rock glaciers in the French Alps based on SPOT-6 orthoimages.[43] Similar to our study, they identified the majority of rock glaciers (60–70%), with better results for large landforms. They achieved a good TP (89%) but with a large number of FPs (21%). We expect that a better resolution would also improve our classification results, especially for small rock glaciers. The automated classification overestimates the total rock glacier area by 243.0%. FPs are located on relict rock glaciers, debris-covered glaciers, and in the glacial foreland. The pixel-based algorithm we employ is not able to identify larger patterns, such as the ridge-and-furrow structure of rock glaciers. This leads to a large number of FPs on landforms with similar pixel properties as rock glaciers, such as debris-covered glacier or creeping debris-covered slopes. We identified 18 additional rock glaciers after comparing the automated classification to the manual outlines. These results indicate that the automated classification is a useful tool to help the analyst but it cannot replace their expertise. Rock glaciers should still be outlined manually. The automated classification identifies areas where the presence of a rock glacier is likely and helps to generate a more complete inventory.

6 | CONCLUSIONS

We combine an automated classification approach with manual outlines to create the first rock glacier inventory of the western Nyainqêntanglha Range on the Tibetan Plateau. We identified 1,433 rock glaciers; 65.9% are classified as transitional and 18.5% as active. The activity of the remaining 15.6% of rock glaciers is undefined, as InSAR displays poor sensitivity to downslope motion in those areas. This classification is based on their median velocities of 2016 to 2019 derived from Sentinel-1 time series analysis. The automated classification correctly identified 87.8% of all rock glaciers at a true positive rate of 69.5% and a false positive rate of 10.4%. Eighteen additional rock glaciers were added to the inventory after reviewing the automated classification results. We conclude that the automated classification is useful to generate a complete inventory but cannot replace the manual outlining process. Rock glaciers on the southern (windward) side of the mountain range are more numerous, distributed over a greater range of elevations, and are more active. Higher moisture availability from monsoon precipitation on the southern side may be the cause of this. However, a more detailed analysis of rock glacier geomorphology is required to corroborate this assumption.

ACKNOWLEDGEMENTS

We would like to thank the DLR for providing us with the high-resolution TanDEM-X DEM for our data processing (Proposal ID DEM_HYDR1727) and the ESA and the Copernicus program for making Sentinel-1 and Sentinel-2 data freely available to the public. We thank our Chinese colleagues, who have worked tirelessly to support us before and during our field work. We also thank Michaela Tille for her work to identify and outline rock glaciers. We thank also Xavier Bodin and the anonymous reviewers for reviewing our manuscript, as well as the editor of *Permafrost and Periglacial Processes*. We are especially grateful to the Open Access Publication Funds of the Technische Universität Braunschweig. This research is a contribution to the International Research Training Group "Geo-ecosystems in transition on the Tibetan Plateau" (TransTiP), funded by Deutsche Forschungsgemeinschaft (DFG grant 317,513,741/GRK 2309).

CONFLICT OF INTEREST

The authors declare no conflicts of interest.

DATA AVAILABILITY STATEMENT

The rock glacier inventory is available on the Pangaea database at https://doi.org/10.1594/PANGAEA.928971. Examples of different rock glaciers in the study area, the outlines of the free ice areas of glaciers, and data related to the downslope velocity of all rock glaciers are included in the Supporting Information of this paper.

ORCID

Eike Reinosch https://orcid.org/0000-0003-3715-0048

REFERENCES

1. Barsch D. *Rock glaciers. Indicators for the present and former geoecology in high mountain environments*. Berlin, Germany: Springer; 1996.
2. French HM. *The periglacial environment*. 4thed. Chichester, UK, and Hoboken, NJ: John Wiley and Sons; 2017.
3. Haeberli W, Hallet B, Arenson L, et al. Permafrost creep and rock glacier dynamics. *Permafr Periglac Process*. 2006;17(3):189-214.
4. Jones DB, Harrison S, Anderson K, Betts RA. Mountain rock glaciers contain globally significant water stores. *Sci Rep*. 2018;8(1):1-10.
5. Azócar GF, Brenning A. Hydrological and geomorphological significance of rock glaciers in the dry Andes, Chile (27–33 S). *Permafr Periglac Process*. 2010;21(1):42-53.
6. Rangecroft S, Harrison S, Anderson K. Rock glaciers as water stores in the Bolivian Andes: an assessment of their hydrological importance. *Arct Antarct Alp Res*. 2015;47(1):89-98.
7. Villarroel CD, Tamburini Beliveau G, Forte AP, Monserrat O. DInSAR for a regional inventory of active rock glaciers in the dry Andes mountains of Argentina and Chile with sentinel-1 data. *Rem Sens*. 2018; 10(10):1588.
8. Halla C, Blöthe JH, Baldis CT, et al. Ice content and interannual water storage changes of an active rock glacier in the dry Andes of Argentina. *Cryosphere*. 2021;15(2):1187-1213.
9. Millar CI, Westfall RD, Delany DL. Thermal and hydrologic attributes of rock glaciers and periglacial talus landforms: Sierra Nevada, California, USA. *Quat Inter*. 2013;310:169-180.

10. Anderson RS, Anderson LS, Armstrong WH, Rossi MW, Crump SE. Glaciation of alpine valleys: The glacier–debris-covered glacier–rock glacier continuum. *Geomorphology*. 2018;311:127-142.
11. Brighenti S, Tolotti M, Bruno MC, Wharton G, Pusch MT, Bertoldi W. Ecosystem shifts in Alpine streams under glacier retreat and rock glacier thaw: A review. *Sci Total Environ*. 2019;675:542-559.
12. Jones DB, Harrison S, Anderson K, Whalley WB. Rock glaciers and mountain hydrology: A review. *Earth Sci Rev*. 2019;193:66-90.
13. Ran Z, Liu G. Rock glaciers in Daxue Shan, south-eastern Tibetan Plateau: an inventory, their distribution, and their environmental controls. *Cryosphere*. 2018;12(7):2327-2340.
14. Scotti R, Brardinoni F, Alberti S, Frattini P, Crosta GB. A regional inventory of rock glaciers and protalus ramparts in the central Italian Alps. *Geomorphology*. 2013;186:136-149.
15. Colucci RR, Forte E, Žebre M, Maset E, Zanettini C, Guglielmin M. Is that a relict rock glacier? *Geomorphology*. 2019;330:177-189.
16. Eriksen HØ, Rouyet L, Lauknes TR, et al. Recent acceleration of a rock glacier complex, Adjet, Norway, documented by 62 years of remote sensing observations. *Geophys Res Lett*. 2018;45(16):8314-8323.
17. Necsoiu M, Onaca A, Wigginton S, Urdea P. Rock glacier dynamics in Southern Carpathian Mountains from high-resolution optical and multi-temporal SAR satellite imagery. *Remote Sens Environ*. 2016;177:21-36.
18. Kääb A, Strozzi T, Bolch T, et al. Inventory and changes of rock glacier creep speeds in Ile Alatau and Kungöy Ala-Too, northern Tien Shan, since the 1950s. *Cryosphere*. 2021;15(2):927–949.
19. Scotti R, Crosta GB, Villa A. Destabilisation of creeping Permafrost: the plator rock glacier case study (Central Italian Alps). *Permafr Periglac Process*. 2017;28(1):224-236.
20. Marcer M, Serrano C, Brenning A, Bodin X, Goetz J, Schoeneich P. Evaluating the destabilization susceptibility of active rock glaciers in the French Alps. *Cryosphere*. 2019;13(1):141-155.
21. Cuo L, Zhang Y. Spatial patterns of wet season precipitation vertical gradients on the Tibetan Plateau and the surroundings. *Sci Rep*. 2017;7(1):1-10.
22. Kang S, Xu Y, You Q, Flügel WA, Pepin N, Yao T. Review of climate and cryospheric change in the Tibetan Plateau. *Environ Res Lett*. 2010;5(1):015101.
23. Berthling I. Beyond confusion: Rock glaciers as cryo-conditioned landforms. *Geomorphology*. 2011;131(3–4):98-106.
24. Knight J, Harrison S, Jones DB. Rock glaciers and the geomorphological evolution of deglacierizing mountains. *Geomorphology*. 2019;324:14-24.
25. Bolch T, Gorbunov AP. Characteristics and origin of rock glaciers in northern Tien Shan (Kazakhstan/Kyrgyzstan). *Permafr Periglac Process*. 2014;25(4):320-332.
26. Lilleøren KS, Etzelmüller B. A regional inventory of rock glaciers and ice-cored moraines in Norway. *Geograf Ann Ser A: Phys Geo*. 2011;93(3):175-191.
27. Monnier S, Kinnard C. Reconsidering the glacier to rock glacier transformation problem: New insights from the central Andes of Chile. *Geomorphology*. 2015;238:47-55.
28. Burger KC, Degenhardt JJ, Giardino JR. Engineering geomorphology of rock glaciers. *Geomorphology*. 1999;31(1-4):93-132.
29. Kääb A, Frauenfelder R, Roer I. On the response of rockglacier creep to surface temperature increase. *Global Planet Change*. 2007;56(1-2):172-187.
30. Kellerer-Pirklbauer A, Kaufmann V. About the relationship between rock glacier velocity and climate parameters in central Austria. *Aust J Ear Sci*. 2012;105(2):94-112.
31. Kenner R, Pruessner L, Beutel J, Limpach P, Philips M. How rock glacier hydrology, deformation velocities and ground temperatures interact: Examples from the Swiss Alps. *Permafr Periglac Process*. 2020;31(1):3-14.
32. Cicoira A, Beutel J, Faillettaz J, Vieli A. Water controls the seasonal rhythm of rock glacier flow. *Earth Planet Sci Lett*. 2019;528:115844.
33. Sorg A, Kääb A, Roesch A, Bigler C, Stoffel M. Contrasting responses of Central Asian rock glaciers to global warming. *Sci Rep*. 2015;5:1-6.
34. Wirz V, Gruber S, Purves RS. Short-term velocity variations at three rock glaciers and their relationship with meteorological conditions. *Earth Surf Dyn*. 2016;4(1):103-123.
35. Strozzi T, Caduff R, Jones N, et al. Monitoring rock glacier kinematics with satellite synthetic aperture radar. *Rem Sens*. 2020;12(3):559.
36. Brardinoni F, Scotti R, Sailer R, Mair V. Evaluating sources of uncertainty and variability in rock glacier inventories. *Earth Surf Process Landf*. 2019;44(12):2450-2466.
37. Crosetto M, Monserrat O, Cuevas-González M, Devanthéry N, Crippa B. Persistent scatterer interferometry: A review. *ISPRS J Photo Rem Sens*. 2016;115:78-89.
38. Delaloye R, Barboux C, Bodin X, et al. Rock glacier inventories and kinematics: A new IPA Action Group. Proc 5th Europ Conf Perm. 2018;23.
39. IPA Action Group: Rock glacier inventories and kinematics. Universität Freiburg Web site. https://www3.unifr.ch. Accessed November 13, 2020.
40. Brenning A. Benchmarking classifiers to optimally integrate terrain analysis and multispectral remote sensing in automatic rock glacier detection. *Remote Sens Environ*. 2009;113(1):239-247.
41. Brenning A, Long S, Fieguth P. Detecting rock glacier flow structures using Gabor filters and IKONOS imagery. *Remote Sens Environ*. 2012;125:227-237.
42. Robson BA, Bolch T, MacDonell S, Hölbling D, Rastner P, Schaffer N. Automated detection of rock glaciers using deep learning and object-based image analysis. *Remote Sens Environ*. 2020;250:112033.
43. Marcer M. Rock glaciers automatic mapping using optical imagery and convolutional neural networks. *Permafr Periglac Process*. 2020;31(4):561-566.
44. Kofler C, Steger S, Mair V, Zebisch M, Comiti F, Schneiderbauer S. An inventory-driven rock glacier status model (intact vs. relict) for South Tyrol, Eastern Italian Alps. *Geomorphology*. 2020;350:106887.
45. Wang X, Liu L, Zhao L, Wu T, Li Z, Liu G. Mapping and inventorying active rock glaciers in the northern Tien Shan of China using satellite SAR interferometry. *Cryosphere*. 2017;11(2):997-1014.
46. Barboux C, Delaloye R, Lambiel C. Inventorying slope movements in an Alpine environment using DInSAR. *Earth Surf Process Landf*. 2014;39(15):2087-2099.
47. Liu L, Millar CI, Westfall RD, Zebker HA. Surface motion of active rock glaciers in the Sierra Nevada, California, USA: inventory and a case study using InSAR. *Cryosphere*. 2013;7(4):1109-1119.
48. Strozzi T, Kääb A, Frauenfelder R. Detecting and quantifying mountain permafrost creep from in situ inventory, space-borne radar interferometry and airborne digital photogrammetry. *Inter J Rem Sens*. 2004;25(15):2919-2931.
49. Wünnemann B, Yan D, Andersen N, et al. A 14 ka high-resolution δ18O lake record reveals a paradigm shift for the process-based reconstruction of hydroclimate on the northern Tibetan Plateau. *Quat Sci Rev*. 2018;200:65-84.
50. Jarvis A, Reuter HI, Nelson A, Guevara E. Hole-filled SRTM for the globe Version 4, International Centre for Tropical Agriculture (CIAT). (http://srtm.csi.cgiar.org Accessed: July 29, 2019). 2008.
51. Keil A, Berking J, Mügler I, Schütt B, Schwalb A, Steeb P. Hydrological and geomorphological basin and catchment characteristics of Lake Nam Co, South-Central Tibet. *Quat Int*. 2010;218(1-2):118-130.
52. Zhang G, Li J, Zheng G. Lake-area mapping in the Tibetan Plateau: an evaluation of data and methods. *Int J Remote Sens*. 2017;38(3):742-772.

53. Yao T, Masson-Delmotte V, Gao J, et al. A review of climatic controls on $\delta^{18}O$ in precipitation over the Tibetan Plateau: Observations and simulations. *Rev Geophys*. 2013;51(4):525-548.
54. Bolch T, Yao T, Kang S, et al. A glacier inventory for the western Nyainqentanglha Range and the Nam Co Basin, Tibet, and glacier changes 1976–2009. *Cryosphere*. 2010;4(3):419-433.
55. Anslan S, Rad MA, Buckel J, et al. Reviews and syntheses: How do abiotic and biotic processes respond to climatic variations in the Nam Co catchment (Tibetan Plateau)? *Biogeoscience*. 2020;17(5):1261-1279.
56. Zhang G, Kang S, Fujita K, et al. Energy and mass balance of Zhadang glacier surface, central Tibetan Plateau. *J Glaciol*. 2013;59(213):137-148.
57. Wang X, Siegert F, Zhou AG, Franke J. Glacier and glacial lake changes and their relationship in the context of climate change, Central Tibetan Plateau 1972–2010. *Global Planet Change*. 2013;111:246-257.
58. Ren S, Menenti M, Jia L, Zhang J, Zhang J, Li X. Glacier mass balance in the Nyainqentanglha Mountains between 2000 and 2017 retrieved from ZiYuan-3 stereo images and the SRTM DEM. *Rem Sens*. 2020;12(5):864.
59. Neckel N, Kropáček J, Bolch T, Hochschild V. Glacier mass changes on the Tibetan Plateau 2003–2009 derived from ICESat laser altimetry measurements. *Environ Res Lett*. 2014;9(1):014009.
60. Li B, Zhang J, Yu Z, Liang Z, Chen L, Acharya K. Climate change driven water budget dynamics of a Tibetan inland lake. *Global Planet Change*. 2017;150:70-80.
61. Zhu L, Xie M, Wu Y. Quantitative analysis of lake area variations and the influence factors from 1971 to 2004 in the Nam Co basin of the Tibetan Plateau. *Chin Sci Bull*. 2010;55(13):1294-1303.
62. Lei Y, Yao T, Bird BW, Yang K, Zhai J, Sheng Y. Coherent lake growth on the central Tibetan Plateau since the 1970s: Characterization and attribution. *J Hydrol*. 2013;483:61-67.
63. Luo W, Zhang G, Chen W, Xu F. Response of glacial lakes to glacier and climate changes in the western Nyainqentanglha range. *Sci Total Environ*. 2020;735:139607.
64. Li Z, Zhao R, Hu J, et al. InSAR analysis of surface deformation over permafrost to estimate active layer thickness based on one-dimensional heat transfer model of soils. *Sci Rep*. 2015;5(1):15542.
65. Reinosch E, Buckel J, Dong J, Gerke M, Baade J, Riedel B. InSAR time series analysis of seasonal surface displacement dynamics on the Tibetan Plateau. *Cryosphere*. 2020;14(5):1633-1650.
66. Zou D, Zhao L, Yu S, et al. A new map of permafrost distribution on the Tibetan Plateau. *Cryosphere*. 2017;11(6):2527-2542.
67. Obu J, Westermann S, Bartsch A. Northern Hemisphere permafrost map based on TTOP modelling for 2000–2016 at 1 km^2 scale. *Earth Sci Rev*. 2019;193:299-316.
68. Tian K, Liu J, Kang S, Li C. A primary study on the environment of frozen ground in the Nam Co Basin, Tibet. *Adv Earth Sci*. 2006;21(12):1324-1332.
69. Buckel J, Reinosch E, Hördt A, et al. Insights into a remote cryosphere: a multi-method approach to assess permafrost occurrence at the Qugaqie basin, western Nyainqêntanglha Range, Tibetan Plateau. *Cryosphere*. 2021;15(1):149-168.
70. Osmanoğlu B, Sunar F, Wdowinski S, Cabral-Cano E. Time series analysis of InSAR data: Methods and trends. *ISPRS J Photo Rem Sens*. 2016;115:90-102.
71. Berardino P, Fornaro G, Lanari R, Sansosti E. A new algorithm for surface deformation monitoring based on small baseline differential SAR interferograms. *IEEE Tran Geosci Rem Sens*. 2002;40(11):2375-2383.
72. Sowter A, Bateson L, Strange P, Ambrose K, Syafiudin MF. DInSAR estimation of land motion using intermittent coherence with application to the South Derbyshire and Leicestershire coalfields. *Remote Sens Lett*. 2013;4(10):979-987.
73. Bateson L, Cigna F, Boon D, Sowter A. The application of the Intermittent SBAS (ISBAS) InSAR method to the South Wales Coalfield, UK. *Int J Appl Ear Obs Geoinf*. 2015;34:249-257.
74. Yagüe-Martínez N, Prats-Iraola P, Gonzalez FR. Interferometric processing of Sentinel-1 TOPS data. *IEEE Tran Geosci Rem Sens*. 2016;54(4):2220-2234.
75. Notti D, Herrera G, Bianchini S, Meisina C, García-Davalillo JC, Zucca F. A methodology for improving landslide PSI data analysis. *Int J Rem Sens*. 2014;35(6):2186-2214.
76. Matsuoka N. Solifluction rates, processes and landforms: a global review. *Earth Sci Rev*. 2001;55(1–2):107-134.
77. Zwieback S, Hensley S, Hajnsek I. Soil moisture estimation using differential radar interferometry: Toward separating soil moisture and displacements. *IEEE Trans Geosci Rem Sens*. 2017;55(9):5069-5083.
78. Cannone N, Gerdol R. Vegetation as an ecological indicator of surface instability in rock glaciers. *Arc Ant Alp Res*. 2003;35(3):384-390.
79. Zhang B, Wu Y, Lei L, et al. Monitoring changes of snow cover, lake and vegetation phenology in Nam Co Lake Basin (Tibetan Plateau) using remote sensing (2000–2009). *J Great Lakes Res*. 2013;39(2):224-233.
80. Zink M, Bachmann M, Brautigam B, et al. TanDEM-X: The new global DEM takes shape. *IEEE Geosci Rem Sens Mag*. 2014;2(2):8-23.
81. Humlum O. Rock glacier types on Disko,Central West Greenland. *Geo Tidss-Dan J Geo*. 1982;82(1):59-66.
82. Hamilton SJ, Whalley WB. Rock glacier nomenclature: A re-assessment. *Geomorphology*. 1995;14(1):73-80.
83. Drusch M, Del Bello U, Carlier S, et al. Sentinel-2: ESA's optical high-resolution mission for GMES operational services. *Remote Sens Environ*. 2012;120:25-36.
84. Otto JC, Prasicek G, Blöthe J, Schrott L. GIS Applications in geomorphology. In: *Comprehensive Geographic Information Systems*; 2018:81-111.
85. Weiss A. Topographic position and landforms analysis. Post Pres ESRI Conf 2001;200.
86. González PJ, Fernández J. Error estimation in multitemporal InSAR deformation time series, with application to Lanzarote, Canary Islands. *J Geophys Res: Solid Earth*. 2011;116(B10):404.
87. Dong J, Zhang L, Liao M, Gong J. Improved correction of seasonal tropospheric delay in InSAR observations for landslide deformation monitoring. *Remote Sens Environ*. 2019;233:111370.
88. Bertone A, Zucca F, Marin C, et al. An unsupervised method to detect rock glacier activity by using Sentinel-1 SAR interferometric coherence: a regional-scale study in the eastern European Alps. *Rem Sens*. 2019;11(14):1711.

SUPPORTING INFORMATION

Additional supporting information may be found online in the Supporting Information section at the end of this article.

How to cite this article: Reinosch E, Gerke M, Riedel B, Schwalb A, Ye Q, Buckel J. Rock glacier inventory of the western Nyainqêntanglha Range, Tibetan Plateau, supported by InSAR time series and automated classification. *Permafrost and Periglac Process*. 2021;1–16. https://doi.org/10.1002/ppp.2117